Sensors and Materials, Vol. 37, No. 8 (2025) 3399–3418
MYU Tokyo

S & M 4125

Damage Diagnosis of Prefabricated Beam Bridges via Multisection Quasistatic Strain Response

Wei Shu,[1] Xiang Zhou,[2] Litao Yu,[1] Chunbin Yu,[1]
Binju Zhang,[1] Faqiang Qiu,[3*] and Yang Liu[2**]

[1]Tongxiang Sutai Expressway Investment and Development Co., Ltd, Tongxiang 314500, China
[2]School of Transportation Science and Engineering, Harbin Institute of Technology, Harbin 150090, China
[3]Jian Yan Test Group Company Limited, Xiamen 361004, China

(Received March 18, 2025; accepted June 19, 2025)

Keywords: prefabricated beam bridge, damage diagnosis, quasistatic influence line, multisection strain response, DPP-BOTDA distributed optical fiber

Distributed optical fibers can effectively overcome an insufficient number of measuring points in structural health monitoring and provide additional measuring point information. However, under quasistatic working conditions, effective solutions for identifying damage in bridge structures with respect to distributed optical fibers are scarce. To address this problem, a structural damage diagnosis method for prefabricated beam bridges, which combines a quasistatic strain influence line with distributed optical fiber sensing technology, is proposed. First, quasistatic strain influence line data for multiple sections of the main beam structure of a bridge are obtained via differential pulse pair–Brillouin optical time-domain analysis technology. By calculating the correlation matrix of the strain response data of different tests, a damage characteristic matrix is constructed, a null space matrix of the damage characteristic matrix is obtained, a damage diagnosis factor is constructed, and a damage judgment threshold is established. Second, by comparing the damage index with the diagnostic threshold under healthy conditions, the location of multisection structural damage can be determined. Considering that structural damage will cause changes in stiffness, the concept of a "strain response area" is introduced, and a quantitative indicator of structural damage is constructed. Last, the proposed method is verified by constructing a scaled-down test model for the multisection damage diagnosis of bridges.

1. Introduction

Bridges and other civil infrastructures play important economic roles.[1–4] Most existing bridge structures are either small- or medium-span bridges.[5,6] After they are built and put into use, small- and medium-span bridges are subject to the multiple effects of self-weight, vehicle loads, and environmental excitations,[7] making them prone to various defects and potential structural damage. If this damage is not maintained and repaired in a timely manner, the service

*Corresponding author: e-mail: qiufaqiang@lets.com
**Corresponding author: e-mail: ly7628@hit.edu.cn
https://doi.org/10.18494/SAM5632

ISSN 0914-4935
https://myukk.org/

life of the bridge will decrease, and the bridge may suddenly collapse, affecting driving and shipping safety. Therefore, ensuring safe bridge operation and the security of life and property by effectively monitoring built bridges, fully understanding actual bridge working conditions, and verifying whether the bearing capacities can meet the strength requirements are critical. To ensure that engineering equipment can work reliably during service, it is particularly important to determine the location and degree of damage. Therefore, structural damage location is a key issue in the field of structural health monitoring.[3,8,9] Characterizing structures based on influence lines is a potential method for identifying bridge damage. Influence lines have been widely used in various bridge engineering applications,[10] such as bridge performance evaluation, dynamic weighing, and model calibration. However, in actual situations, because a moving load always has a certain speed, it is theoretically impossible to obtain static influence lines for operating bridges. In contrast, only quasistatic moving loads, that is, vehicles traveling at a slow and uniform speed, can produce bridge superstructure data. Under the above quasistatic loading conditions, strain approximation static influence lines are used. Liu and Zhang[11] applied Brillouin-optical time-domain analysis (BOTDA) technology to determine quasistatic strain bridge damage locations and considerably increased the number of strain measurement points. The authors propose a damage localization index based on quasistatic strain influence lines and verify that this method can be used for beam bridge superstructure damage localization via numerical analysis and quasistatic test data of a model bridge. Deng *et al.*[12] proposed a damage identification method based on the probability distribution correlation of quasistatic response data and proved that the change in the structural state can be inferred from the change in the probability distribution correlation of multiple quasistatic response data. The displacement movement difference between the two monitored quasistatic responses is used as the damage indicator, and the proposed method is verified via the measured data of a cable-stayed bridge. Zhu *et al.*[13] proposed a quasistatic structural damage identification method based on a single-sensor influence line and empirical Bayesian threshold estimation. The dynamic influence caused by the vehicle was eliminated by preprocessing, and a differential index based on the influence line area was constructed. However, the above research focused only on whether damage occurred, and the various factors that affect the effectiveness of the damage detection method were not fully considered. A situation in which the quasistatic influence line acquisition is relatively simple is possible. Owing to the effect of the number and measurement range of "point" sensors in traditional structural health monitoring,[14] many point sensors must typically be installed to monitor the structural state comprehensively. Moreover, the location of structural damage is even more critical. Optical fibers have good transmission and sensing integration characteristics. An increasing number of researchers are exploring the application of distributed monitoring technology in structural damage identification. Liu *et al.*[15] converted structural strain to a cross-sectional curvature of a tunnel via a BOTDA sensor based on fully distributed Brillouin scattering, which effectively solved the problem of the insufficient sensitivity of strain to structural damage in actual tunnel structures, and verified it via an actual box tunnel model. Oskoui *et al.*[16] proposed a method for detecting damage along the length of multispan continuous bridges and verified the effectiveness of the method via a loading test of a five-span continuous prefabricated post-tensioned concrete box girder bridge. Yang *et al.*[17] used

information fusion to establish a strain damage probability index and a strain curvature damage probability index. With the continuous development of computer science, deep learning has been continuously used in structural damage monitoring. Ying *et al.*[18] proposed a new method for locating and quantifying bridge damage by using deep neural networks for multi-objective regression tasks and obtained the final quantitative damage value via statistical analysis. Nguyen-Ngoc *et al.*[19] combined a one-dimensional convolutional neural network with a long short-term memory network and improved it by using symbolic aggregation approximation for time series data analysis. The enhancement and transformation technology can accurately detect damage to a bridge structure. In the above methods, owing to the number and density of measurement points, low monitoring accuracy can result, especially when the degree of damage is small or large, which will produce nonnegligible errors.

The traditional BOTDA system[14,20,21] is limited by a phonon lifetime of 10 ns, and the spatial resolution cannot exceed 1 m. When the pulse width is less than the phonon lifetime (10 ns, corresponding to 1 m spatial resolution), the Brillouin gain spectrum broadens rapidly above 100 MHz, making it more difficult to maintain the accuracy of the measured Brillouin frequency shift.[22] With differential pulse pair (DPP) technology,[23,24] two long-pulse Brillouin time domain signals with a pulse width difference of less than 10 ns can be differentiated to achieve centimeter-level spatial resolution. In addition, by using two long pulses as pump pulses, the obtained sampling spectrum width is near the Brillouin eigenspectral width, which enables better frequency resolution. Compared with other technologies, DPP-BOTDA requires no modification of the system structure and only simple data processing, making it a good method for increasing spatial resolution.[25]

On the basis of the quasistatic load test method and full-scale BOTDA technology, we constructed a correlation function matrix between the strain response data of each loading condition, established a zero-space matrix of the correlation function matrix in the healthy state of the bridge, constructed a damage diagnosis factor for the bridge structure on the basis of abnormal diagnosis, and then proposed a multisection damage discrimination and damage area positioning algorithm for the bridge. Moreover, based on the successful diagnosis of bridge structural damage, an equivalent reduction factor of the overall stiffness of the damaged structure was proposed using the area ratio of the strain influence line before and after damage to the bridge structure under quasistatic loading to quantify the damage to the bridge structure. Finally, the proposed algorithm was verified via a scaled simply supported beam model.

2. Brillouin-optical Tme-domain Analysis-based Monitoring Algorithm Theory

DPP-BOTDA is a BOTDA sensing technology based on DPP technology. The technology uses two pump pulses with pulse widths of t1 and t3 to be sequentially incident into the optical fiber at an interval of t2 (>2 nL/c). Similarly, the Brillouin scattered light generated by the interaction with the continuous light is received by the detector, and the Brillouin signals corresponding to the two pulses are collected and then subtracted in the time domain. After the Brillouin gain spectrum of each point in the optical fiber is acquired via frequency scanning, the Brillouin frequency shift of each point is obtained via curve fitting; that is, the temperature and strain are obtained by demodulating the difference Brillouin signal, as shown in Fig. 1.

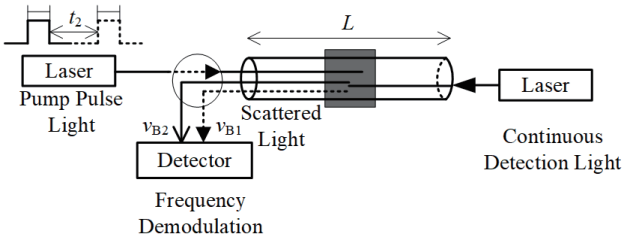

Fig. 1. Schematic of differential pulse pair technology.

2.1 Monitoring principle of Brillouin-optical time-domain analysis

BOTDA uses optical time domain positioning technology to calculate the time difference between the Stokes light generated by stimulated Brillouin scattering and the pump light to achieve the correspondence between each time point and the optical fiber position z:

$$z = \frac{c\tau}{2n}, \tag{1}$$

where c represents the speed of light in a vacuum, τ represents the pump pulse width, and n represents the fiber refractive index.

$$v_a = \sqrt{\frac{E(1-k)}{\rho(1+k)(1-2k)}} \tag{2}$$

Here, v_a represents velocity of sound, E represents the elastic modulus of the optical fiber medium, k represents Poisson's ratio of the optical fiber medium, and ρ represents the fiber medium density.

Because E, k, ρ, and n are affected by strain and temperature, they can be expressed as functions of strain and temperature, and we obtain

$$\begin{aligned} v_B &= 2nv_a/\lambda_p = v_B(\varepsilon,T) \\ &= 2n(\varepsilon,T)\sqrt{\frac{E(\varepsilon,T)(1-k(\varepsilon,T))}{\rho(\varepsilon,T)(1+k(\varepsilon,T))(1-2k(\varepsilon,T))}}\Big/\lambda_p . \end{aligned} \tag{3}$$

Owing to the elastomeric effect, strain changes the refractive index by modulating the Poisson's ratio μ and the elastic modulus E of the optical fiber, thereby causing a change in the Brillouin frequency shift. Under the condition of constant temperature ($T = 0$), the change in the Brillouin frequency shift with strain is analyzed, and Eq. (3) is rewritten as

$$v_B(\varepsilon,0) = 2n(\varepsilon,0)\sqrt{\frac{E(\varepsilon,0)(1-k(\varepsilon,0))}{\rho(\varepsilon,0)(1+k(\varepsilon,0))(1-2k(\varepsilon,0))}}\Big/\lambda_p . \tag{4}$$

At the initial strain, the Taylor series formula is expanded for Eq. (4), and the first-order terms are retained. The second-order and above terms can be disregarded because they are on the order of microstrain. Then the following equation is obtained:

$$\begin{aligned} v_B(\varepsilon,0) &= v_B(\varepsilon_0,0)+v_B{}'(\varepsilon_0,0)(\varepsilon-\varepsilon_0) \\ &= v_B(\varepsilon_0,0)[1+\frac{v_B{}'(\varepsilon_0,0)}{v_B(\varepsilon_0,0)}(\varepsilon-\varepsilon_0)], \end{aligned} \tag{5}$$

where v_B represents the Bridgman frequency, $\frac{v_B{}'(\varepsilon_0,0)}{v_B(\varepsilon_0,0)}$ represents the derivative function related to ε. By introducing the strain influence coefficient $C_\varepsilon = \frac{v_B{}'(\varepsilon_0,0)}{v_B(\varepsilon_0,0)}$ of the Brillouin frequency shift v_B, Eq. (5) is simplified to

$$v_B(\varepsilon,0) = v_B(\varepsilon_0,0)(1+C_\varepsilon\Delta\varepsilon). \tag{6}$$

The thermo-optic effect is the way in which temperature affects the refractive index of optical fibers, and the thermal expansion effect is the way in which temperature affects the density of optical fibers. In addition, the free energy of the optical fiber changes with temperature, thus causing changes in the Poisson's ratio and elastic modulus, which cause changes in the Brillouin frequency shift. Under the premise that the strain remains constant (= 0), the change in the Brillouin frequency shift with temperature is analyzed, and Eq. (3) is expressed as

$$v_B(0,T) = 2n(0,T)\sqrt{\frac{E(0,T)(1-k(0,T))}{\rho(0,T)(1+k(0,T))(1-2k(0,T))}}\Big/\lambda_p . \tag{7}$$

At the initial temperature, Eq. (7) is expanded according to Taylor expansion, and the first-order terms are retained to obtain

$$\begin{aligned} v_B(0,T) &= v_B(0,T_0)+v_B{}'(0,T_0)(T-T_0) \\ &= v_B(0,T_0)[1+\frac{v_B{}'(0,T_0)}{v_B(0,T_0)}(T-T_0)]. \end{aligned} \tag{8}$$

By introducing the temperature effect coefficient of the Brillouin frequency shift $C_T = \frac{v_B{}'(0,T_0)}{v_B(0,T_0)}$, Eq. (8) is simplified to

$$v_B(0,T) = v_B(\varepsilon_0,T_0) + C_\varepsilon\Delta\varepsilon + C_T\Delta T. \tag{9}$$

By combining Eqs. (6) and (9), we establish a linear relationship among the Brillouin frequency shift, strain, and temperature.

$$v_B(\varepsilon,T) = v_B(\varepsilon_0,T_0) + C_\varepsilon \Delta\varepsilon + C_T \Delta T \tag{10}$$

The bridge structural damage diagnosis method, which is based on the multisection strain response, is based on quasistatic loading. The following describes the quasistatic loading process.

The loading vehicle passes over the bridge slowly at a constant speed. When the vehicle reaches a position at a distance Z_i from one end of the bridge, according to the data processing specifications of BOTDA technology, the relative strains $\Delta\varepsilon_1$, $\Delta\varepsilon_2$, ..., $\Delta\varepsilon_q$ under a certain reference state can be obtained at strain collection points $1 - q$ to acquire "distance–strain" through sensors to construct quasistatic strain influence lines.

By loading position j, with the relative strain $\Delta\varepsilon$ as the vertical axis and the strain measurement point number as the horizontal axis, and by smoothly connecting the relative strain values $\Delta\varepsilon_p$, a continuous relationship curve of "$\Delta\varepsilon - x$", namely, the "relative strain–measurement point position" curve, is constructed. This quasistatic strain response curve, which is hereinafter referred to as the quasistatic strain response, is shown in Fig. 2.

By analyzing the health status of the bridge and the changes in the quasistatic strain response under the condition to be diagnosed, the damage condition can be determined. On this basis, a rapid bridge damage diagnosis algorithm based on a quasistatic multisection strain response, which can determine whether a structure is damaged, the location of the damage, and the degree of damage, is proposed.

2.2 Damage diagnosis of prefabricated beam bridge via multisection strain response

Compared with displacement influence line damage diagnosis via traditional "point" distributed sensors, the damage diagnosis algorithm, which is based on strain collection via DPP-BOTDA technology, has high spatial resolution and high measurement accuracy. By analyzing the strain variations in the local area before and after the bridge structure is damaged, the damage judgment can be completed, and the damage in the area can be located.

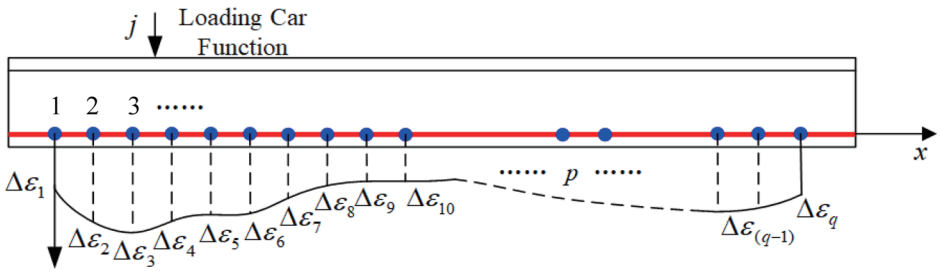

Fig. 2. (Color online) Schematic of quasistatic strain response.

2.2.1 Generation of the damage judgment threshold of a bridge

To establish quasistatic loading, n tests under the same working conditions, which are referred to as "a group", are performed. In each group of experiments, the strain data obtained during each interval are subtracted from the average value of the strain data of the relaxation segment of the fiber:

$$\boldsymbol{\omega}_i^i = \boldsymbol{\omega}_{io}^i - \boldsymbol{\varepsilon}_{mean}, \tag{11}$$

where $\boldsymbol{\omega}_i^i$ represents the strain vector after the ith test treatment at measurement point i, $\boldsymbol{\omega}_{io}^i$ represents the original measurement data, and $\boldsymbol{\varepsilon}_{mean}$ is the average value of the strain data of the optical fiber relaxation section.

The first loading position "1" of the vehicle is selected as an example; n experiments are conducted in succession; the strain response data are recorded as $\boldsymbol{\omega}_1^1, \boldsymbol{\omega}_1^2, \cdots, \boldsymbol{\omega}_1^n$; the column vector data at "2" are recorded as $\boldsymbol{\omega}_2^1, \boldsymbol{\omega}_2^2, \cdots, \boldsymbol{\omega}_2^n$; the strain response data at position j are recorded as $\boldsymbol{\omega}_j^1, \boldsymbol{\omega}_j^2, \boldsymbol{\omega}_j^3, \cdots \boldsymbol{\omega}_j^n$; the loading position "1" is used as a reference; and the damage characteristic matrix is constructed by calculating the correlation matrix of the strain response data of different tests:

$$\overline{\mathbf{H}}^1 = \begin{bmatrix} \operatorname{cov}(\{\boldsymbol{\omega}_1^1\},\{\boldsymbol{\omega}_1^1\}) & \operatorname{cov}(\{\boldsymbol{\omega}_1^1\},\{\boldsymbol{\omega}_1^2\}) & \cdots & \operatorname{cov}(\{\boldsymbol{\omega}_1^1\},\{\boldsymbol{\omega}_1^n\}) \\ \operatorname{cov}(\{\boldsymbol{\omega}_1^1\},\{\boldsymbol{\omega}_2^1\}) & \operatorname{cov}(\{\boldsymbol{\omega}_1^1\},\{\boldsymbol{\omega}_2^2\}) & \cdots & \operatorname{cov}(\{\boldsymbol{\omega}_1^1\},\{\boldsymbol{\omega}_2^n\}) \\ \vdots & \vdots & \vdots & \vdots \\ \operatorname{cov}(\{\boldsymbol{\omega}_1^1\},\{\boldsymbol{\omega}_j^1\}) & \operatorname{cov}(\{\boldsymbol{\omega}_1^1\},\{\boldsymbol{\omega}_j^2\}) & \cdots & \operatorname{cov}(\{\boldsymbol{\omega}_1^1\},\{\boldsymbol{\omega}_j^n\}) \end{bmatrix}_{j\times n}. \tag{12}$$

By performing singular value decomposition on the $\overline{\mathbf{H}}^1$ matrix, we obtain

$$\overline{\mathbf{H}}^1 = \overline{\mathbf{U}}^1 \cdot \overline{\mathbf{S}}^1 \cdot (\overline{\mathbf{V}}^1)^{\mathrm{T}}, \tag{13}$$

where $\overline{\mathbf{S}}^1$ represents a semipositive $j \times n$ diagonal matrix and $(\overline{\mathbf{V}}^1)^{\mathrm{T}}$ represents the conjugate transpose of $\overline{\mathbf{V}}$, which is an $n \times n$-order unitary matrix. The conjugate transpose of a unitary matrix is equal to its inverse matrix; $\overline{\mathbf{U}}^1$ is a $j \times j$-order unitary matrix. There exists a matrix $\mathbf{t}$ such that

$$\mathbf{t} \cdot \overline{\mathbf{H}}^1 = \mathbf{0}. \tag{14}$$

Let

$$\overline{\boldsymbol{\xi}}_h^1 = \operatorname{norm}(\mathbf{t} \cdot \overline{\mathbf{H}}^1), \tag{15}$$

where the norm(•) represents the Euclidean norm of the matrix.

$\mathbf{t}\cdot\overline{\mathbf{H}}^{1}$ is not actually a zero matrix, so its norm $\overline{\xi}_h^1$ is the damage index at loading position "1". At loading position "2", the damage characteristic matrix is constructed with $\boldsymbol{\omega}_2^1$ as a reference:

$$\overline{\mathbf{H}}^{2}=\begin{bmatrix}\operatorname{cov}(\{\boldsymbol{\omega}_1^1\},\{\boldsymbol{\omega}_1^1\}) & \operatorname{cov}(\{\boldsymbol{\omega}_1^1\},\{\boldsymbol{\omega}_1^2\}) & \cdots & \operatorname{cov}(\{\boldsymbol{\omega}_1^1\},\{\boldsymbol{\omega}_1^n\})\\ \operatorname{cov}(\{\boldsymbol{\omega}_1^1\},\{\boldsymbol{\omega}_2^1\}) & \operatorname{cov}(\{\boldsymbol{\omega}_1^1\},\{\boldsymbol{\omega}_2^2\}) & \cdots & \operatorname{cov}(\{\boldsymbol{\omega}_1^1\},\{\boldsymbol{\omega}_2^n\})\\ \vdots & \vdots & \vdots & \vdots\\ \operatorname{cov}(\{\boldsymbol{\omega}_1^1\},\{\boldsymbol{\omega}_j^1\}) & \operatorname{cov}(\{\boldsymbol{\omega}_1^1\},\{\boldsymbol{\omega}_j^2\}) & \cdots & \operatorname{cov}(\{\boldsymbol{\omega}_1^1\},\{\boldsymbol{\omega}_j^n\})\end{bmatrix}_{j\times n}. \tag{16}$$

Using Eq. (16), the null space of the $\overline{\mathbf{H}}^{2}$ matrix can be obtained as

$$\overline{\xi}_h^2=\operatorname{norm}(\mathbf{t}\cdot\overline{\mathbf{H}}^{2}). \tag{17}$$

The damage characteristic matrix is constructed at each loading position to obtain the damage diagnosis index. Therefore, at j loading positions, j damage indices up to $\overline{\xi}_h^j=\operatorname{norm}(\mathbf{t}\cdot\overline{\mathbf{H}}^{j})$ can be obtained. By continuing to carry out f groups of tests, each loading position yields f damage indicators, and damage diagnosis thresholds $\overline{\eta_1}\sim\overline{\eta}_j$ can be established for each.

The set of damage diagnostic indicators under healthy conditions is defined as ξ_h. After the set of injury characteristics under healthy conditions is obtained, the threshold is constructed by selecting the 5% percentile from the set.

$$\eta_i=\partial_i\{\xi_h\}_{95\%} \tag{18}$$

Here, ∂_i represents the guarantee coefficient of the basic model of steady-state data, which is usually 1.2, and $\{\bullet\}_{95\%}$ indicates the values at the last 5% positions within this set.

We have introduce the concept of hypothesis testing. The null hypothesis H_0 indicates that no damage has occurred to the structure. The alternative hypothesis H_1 indicates that the structure has already suffered damage. Then, the damage assessment process is as follows: if $\overline{\xi}_{\mathrm{DA}}^{i}<\overline{\eta}_i$, accept the null hypothesis H_0, which states that the structure is not damaged; if $\overline{\xi}_{\mathrm{DA}}^{i}>\overline{\eta}_i$, then reject H_0, which implies that the structure has suffered damage.

2.2.2 Damage location of the bridge

We find "1~j" under damage condition A of a certain working condition to be diagnosed. Then, we obtain the damage index of the "1~j" loading position under a certain working condition A $\overline{\xi}_{\mathrm{DA}}^{1}\sim\overline{\xi}_{\mathrm{DA}}^{j}$, and carry out multiple quasistatic load tests. n tests are conducted under Damage Condition A, the strain response data at loading position "1" are recorded as $\boldsymbol{\omega}(\mathrm{A})_1^1,\boldsymbol{\omega}(\mathrm{A})_1^2,\boldsymbol{\omega}(\mathrm{A})_1^3,\cdots\boldsymbol{\omega}(\mathrm{A})_1^n$, as shown in Eq. (11), and the damage characteristic matrix is constructed with the strain response data under healthy conditions:

$$\overline{\mathbf{H}}(\mathrm{A})=\begin{bmatrix} \mathrm{cov}(\{\boldsymbol{\omega}_1^1\},\{\boldsymbol{\omega}_1^1\}) & \mathrm{cov}(\{\boldsymbol{\omega}_1^1\},\{\boldsymbol{\omega}_1^2\}) & \cdots & \mathrm{cov}(\{\boldsymbol{\omega}_1^1\},\{\boldsymbol{\omega}_1^n\}) \\ \mathrm{cov}(\{\boldsymbol{\omega}_1^1\},\{\boldsymbol{\omega}_2^1\}) & \mathrm{cov}(\{\boldsymbol{\omega}_1^1\},\{\boldsymbol{\omega}_2^2\}) & \cdots & \mathrm{cov}(\{\boldsymbol{\omega}_1^1\},\{\boldsymbol{\omega}_2^n\}) \\ \vdots & \vdots & \vdots & \vdots \\ \mathrm{cov}(\{\boldsymbol{\omega}_1^1\},\{\boldsymbol{\omega}_j^1\}) & \mathrm{cov}(\{\boldsymbol{\omega}_1^1\},\{\boldsymbol{\omega}_j^2\}) & \cdots & \mathrm{cov}(\{\boldsymbol{\omega}_1^1\},\{\boldsymbol{\omega}_j^n\}) \end{bmatrix}_{j\times n}. \tag{19}$$

Using Eq. (14), we can obtain the null space matrix of **K** via singular value decomposition; then, the damage index at loading position "1" under damage condition A is

$$\overline{\xi}_{\mathrm{DA}}^{1}=\mathrm{norm}(\mathbf{t}\cdot\overline{\mathbf{H}}_{\mathrm{A}}^{1}). \tag{20}$$

Similarly, the damage index $\overline{\xi}_{\mathrm{DA}}^{i}$ of the bridge structure corresponding to loading position "1~*j*" under these working conditions can be obtained. By introducing hypothesis testing, the null hypothesis H_0 indicates that the structure has not been damaged, and the alternative hypothesis H_1 indicates that the structure has been damaged. The damage judgment process is as follows: if $\overline{\xi}_{\mathrm{DA}}^{i}<\overline{\eta}_i$, the null hypothesis H_0 is accepted; if $\overline{\xi}_{\mathrm{DA}}^{i}>\overline{\eta}_i$, H_0 is rejected, and the structure is assumed to have been damaged. The bridge structural damage diagnosis algorithm, which is based on a multisection strain response, can also locate the damaged area; that is, damage occurs at loading position *i*.

Because strain is a local quantity that reflects the structural response, when the loading vehicle is at the damaged position, the resulting strain variation in the damaged area is the largest. This change is reflected in the change in the strain response, thereby causing a change in the damage index. When the damage index exceeds the threshold, the structural damage can be located in the area.

2.2.3 Damage quantification of the bridge

Damage to the bridge structure results in a decrease in the structural elastic modulus. Because the unit area A can reflect the cross-sectional information of the structure, similar to the moment of inertia I, the elastic modulus E and the moment of inertia I are coupled. Therefore, the damage is reflected in the decrease in EI, and the decrease in stiffness is reflected in the change in the quasistatic strain response.

The concept of the "strain response area" is introduced to characterize the change in the quasistatic strain response. The expression at loading position *j* under a certain working condition is

$$S_j=\int_1^q \omega_j(x)_n dx. \tag{21}$$

The above analysis reveals that the change in the strain response reflects a decrease in the stiffness of the bridge structure. Therefore, the strain response area will also change before and

after the bridge structure is damaged. At a certain loading position, the strain response curves before and after structural damage differ, which represents the change in structural stiffness caused by local damage. Therefore, the change in the overall stiffness of the structure can be expressed by analyzing the relative change in the sum of the strain response areas obtained at loading position j before and after damage.

When the structure is subjected to n loading tests in a healthy state (H), at each loading position, n strain response curves can be obtained, which correspond to n strain response areas. To reduce interference factors such as environmental interference and test errors, the strain response areas at each loading position are averaged.

$$\begin{aligned}&\frac{S_j(H)_1+S_j(H)_2\cdots+S_j(H)_n}{n}\\&=\frac{\int_1^q \omega_j(x)_1\,dx+\int_1^q \omega_j(x)_2\,dx\cdots+\int_1^q \omega_j(x)_n\,dx}{n}=\overline{S_j(H)}.\end{aligned} \tag{22}$$

The sum of the areas of all the strain responses obtained at loading position j for the entire bridge under healthy conditions (H) is

$$\overline{S_1(H)}+\overline{S_2(H)}+\cdots\overline{S_i(H)}+\cdots+\overline{S_{(j-1)}(H)}+\overline{S_j(H)}=\sum_{i=1}^{j}\overline{S_i(H)}. \tag{23}$$

When the structure is under the damaged condition (D), the strain response area at loading position j is $S_j(D)=\int_1^q \omega_j(x)dx$; b tests are carried out under this condition, and the average value of b tests is taken as the strain response area at point j.

$$\begin{aligned}&\frac{S_j(D)_1+S_j(D)_2\cdots+S_j(D)_n}{b}\\&=\frac{\int_1^q \omega_j(x)_1\,dx+\int_1^q \omega_j(x)_2\,dx\cdots+\int_1^q \omega_j(x)_n\,dx}{b}=\overline{S_j(D)}\end{aligned} \tag{24}$$

The sum of the strain response areas obtained at loading position j for the entire bridge under damage condition (D) is

$$\overline{S_1(D)}+\overline{S_2(D)}+\cdots\overline{S_i(D)}+\cdots+\overline{S_{(j-1)}(D)}+\overline{S_j(D)}=\sum_{i=1}^{j}\overline{S_i(D)}, \tag{25}$$

where φ is introduced as a quantitative indicator of bridge damage to characterize the degree of structural damage. The expression for the quasistatic strain response is

$$\varphi = 1 - \frac{\sum_{i=1}^{j} \overline{S_i(H)}}{\sum_{i=1}^{j} \overline{S_i(D)}}. \tag{26}$$

After the quantitative index of overall damage is obtained, the degree of damage of the entire structure can be analyzed; that is, quantitative analysis of the damage can be performed.

3. Experimental Verification

On the basis of the basic principles of DPP-BODDA (high-performance distributed Brillouin optical fiber sensing) technology and the bridge multisection damage diagnosis algorithm described in Sect. 2, a test model based on the transverse connection damage failure mode was established. The quasistatic loading system, real-time driving distance monitoring system, and other auxiliary equipment were further designed, and the experimental verification scheme design for the bridge multisection damage diagnosis method was completed. To counteract the influence of temperature and reduce experimental errors, we set up an optical fiber relaxation section that did not come into contact with the beam body. During the experiment, data from both the test section and the relaxation section were collected. By subtracting the strain data of the relaxation section from those of the test section, test data with smaller errors could be obtained. At the same time, in order to avoid any influence of temperature changes, we chose to conduct the experiment in a constant-temperature laboratory and ensure that the entire experiment could be completed within a relatively short period of time.

3.1 Beam bridge test model

Considering the stress conditions of the actual bridge, to make the test model as similar as possible to the actual structure, a scaled-down bridge model with a certain similarity ratio was designed based on of the span and material of the actual bridge. The model was a simply supported beam bridge composed of three aluminum alloy beams, and the cross section is shown in Fig. 3.

The simulation of damage is particularly critical. The test uses a specific damage mode of "bridge transverse connection damage"; that is, the bridge structural damage simulation is achieved by weakening the transverse connection between the beams. The transverse connection between adjacent beams is simulated by "fastening bolts + steel pads", and the steel blocks are located on the lower side of the flange plate.

The bolts are tightened to fit the steel pads to the flange plate to simulate the healthy state, the steel pads are removed, and even the transverse connection is damaged to simulate the damaged condition. The overall stiffness of the bridge structure decreases before and after damage, which results in changes in the structural response. Strain damage is local damage, and reducing the

Fig. 3. (Color online) Overall view of the simulation test bridge model.

number of transverse connection bolts can simulate a small degree of structural damage. The test model is equipped with 22 transverse steel pads, and their positions are shown in Fig. 4.

During the experiment, the displacement of the trolley and the strain response of the data acquisition system are recorded simultaneously, thereby establishing the "displacement–driving" influence line.

3.2 Analysis of abnormal data

Because the optical fiber must be fused with the optical fiber connector before it can be connected to the strain acquisition equipment, the optical fiber layout scheme is considered, as shown in Fig. 5.

To obtain reliable data on the structural response under damage conditions, measurements are taken four or more times each, and the average value of multiple data points is selected as the Brillouin frequency shift data to be processed. The healthy state and three different damage conditions of small, medium, and large damage levels are established. The healthy state is simulated by tightening the bolts to fit the steel pads to the flange plate. The healthy state is the reference state, and the number of tests is 18. The damage simulation is achieved by removing different numbers and positions of transverse connection bolts.

Owing to uneven adhesive application or different degrees of adhesive curing and shrinkage and the need to manually stretch the optical fiber to keep it straight during fiber optic laying, this interference factor causes tensile stress on the optical fiber in some areas, and the tensile stress is not reduced owing to the curing of the adhesive. Therefore, strain maximum points exist in the two initial strain segments ($x1$–$x2$) and ($x3$–$x4$). The information of four measurement points is removed from both ends of each optical fiber to obtain the Brillouin frequency shift data to be processed. The positions of the selected optical fiber data segments on both sides of the beam are shown in Fig. 6.

The relative strain variation under no-load and healthy conditions is very small because the strain variation amplitude of the two measurement cases relative to that of the relaxed fiber is large; however, the relative strain variation amplitude between the two working conditions is small. The damage diagnosis threshold can be established by carrying out multiple loading tests under bridge health conditions and combining it with the theory of bridge structural damage diagnosis algorithms based on multisection strain responses. To obtain more accurate strain

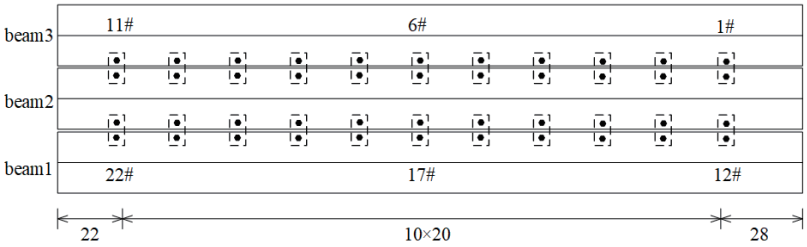

Fig. 4. Transverse connection layout of the full bridge model (unit: cm).

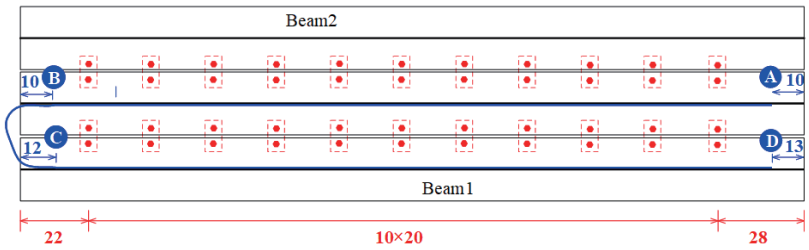

Fig. 5. (Color online) Top view of the optical fiber pasting position (unit: cm).

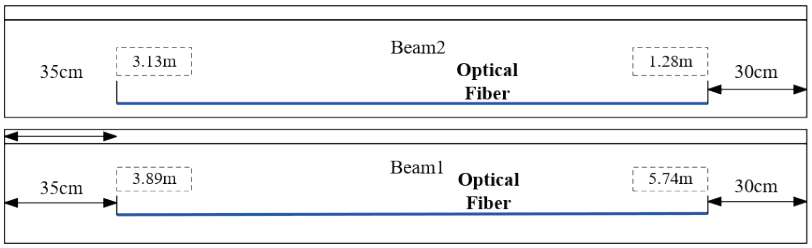

Fig. 6. (Color online) Top view of the fiber paste.

variation data caused by loading, the Brillouin frequency shift data collected during each interval must be subtracted from the data of the fiber in the relaxation section of the test. The strain variation caused by temperature change and the initial strain distribution after excluding environmental influences are shown in Fig. 7. In the figure, point A represents the starting point of the optical fiber on the 2nd beam, point B indicates the starting point for data collection of the 2nd beam's optical fiber, and point C is the end point for data collection on the optical fiber of the 2nd beam. Point D indicates the starting point for data collection of the 1st beam, whereas Point E represents the end point for data collection of the 1st beam. As shown in Fig.7, X1 represents the data calibration section, X2 and X4 represent the fiber data acquisition sections, and X3 represents the fiber relaxation section.

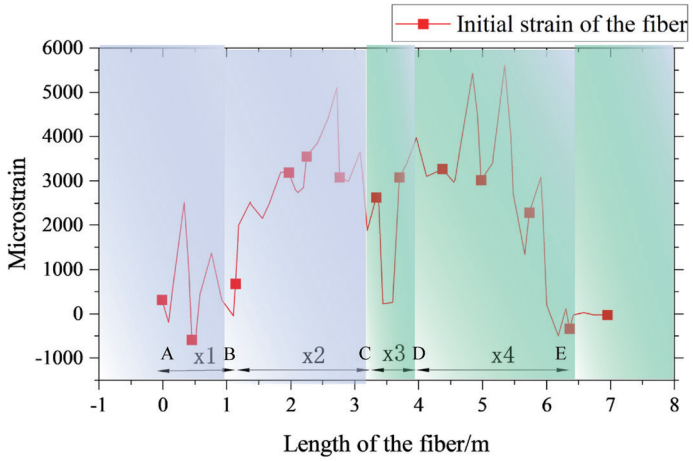

Fig. 7. (Color online) Initial strain distribution of the optical fiber under no load.

4. Results

In this section, the BOTDA frequency shift data under small, medium, and large damage conditions are used to obtain the relative strain. Additionally, the test results are analyzed using the bridge structural damage diagnosis algorithm based on the multisection strain response to evaluate the effectiveness of the algorithm in the process of bridge damage discrimination.

4.1 Damage diagnosis in the case of a small degree of damage

a) Numerical analysis of the bridge structure strain response under Working Condition 1.

Strain data collected before and after damage at the loading position 90 cm from the left end of the bridge on the front wheel of the loading vehicle were selected for analysis. The strain response in the healthy condition is shown in blue, and the strain response in the damaged condition is shown in red.

As seen in Fig. 8, the difference in the relative strain relationship before and after damage to the structure is very small, and it is impossible to determine whether the structure is damaged under damage conditions. Additionally, the change in the strain response cannot be obtained by direct observation, so it is necessary to use a damage diagnosis algorithm for bridge structures based on multisection strain responses to perform damage judgments. Figure 9 shows the recognition results of this algorithm. The results indicate that at loading positions 24 and 25, the damage exceeded the threshold, and structural damage occurred at these two locations.

b) Location and identification results of bridge structural damage in Case 1.

For the small degree of damage case 1, the test data analysis results obtained using the algorithm reveal that the damage diagnosis index of the loading vehicle at positions #24 and #25 exceeds the corresponding damage diagnosis threshold, and the structure can be assumed to be damaged at this position. The algorithm determines that the bridge structure is damaged within the distance range of 5–46 cm from the right end of the bridge, and the #1 lateral connection is within the range of the algorithm prediction of 28 cm from the right end of the bridge. As shown

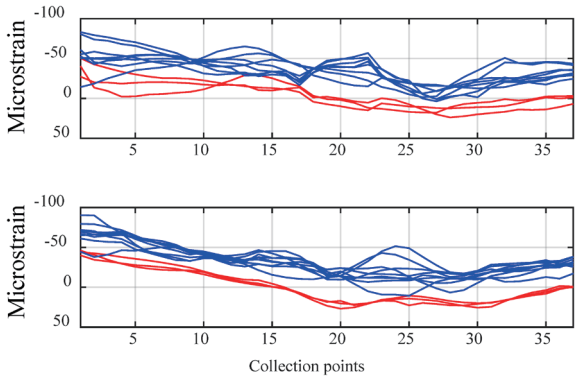

Fig. 8. (Color online) Damage Condition 1: Loading at 90 cm from front wheel.

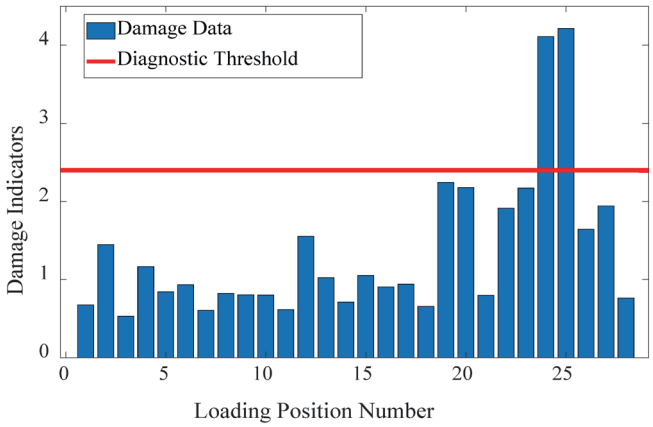

Fig. 9. (Color online) Damage diagnosis results for Damage Condition 1.

in Fig. 10, the shaded part is wherre the algorithm was used to locate the damage area. Therefore, the bridge structural damage diagnosis algorithm, which is based on the multisection strain response, can be used to diagnose and locate events with a small degree of damage in a structure.

c) Quantification of bridge structural damage in Case 1

The change in the strain response area S_j caused by damage reflects the reduction in the stiffness of the bridge structure and can be used to quantify damage. In this experiment, damage quantification is performed, and the strain response area is used to calculate the average value $\overline{S}_j$ of the strain response area at each loading position under one working condition. Then, the 28 $\overline{S}_j$ values are summed to obtain $\sum_{i=1}^{28} \overline{S}_j$ as the characteristic quantity that characterizes the overall stiffness of the bridge structure under these working conditions. Therefore, under Damage Condition 1, the degree of damage to the bridge structure is 4.7%. The results of damage quantification are shown in Fig. 11. Near the damage location, the corresponding variations in the strain response area under the damage conditions are large, and those at other locations are small.

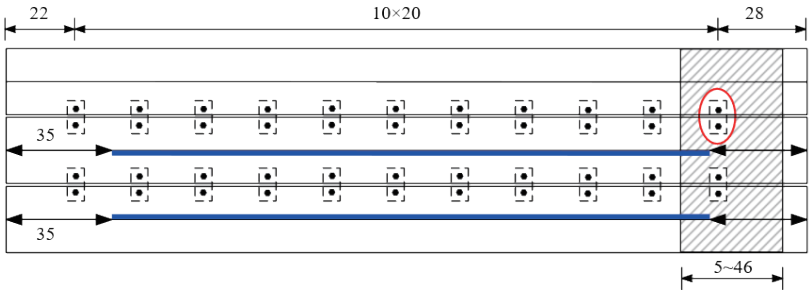

Fig. 10. (Color online) Relationship between damage location and lateral connection position for Working Condition 1 (unit: cm).

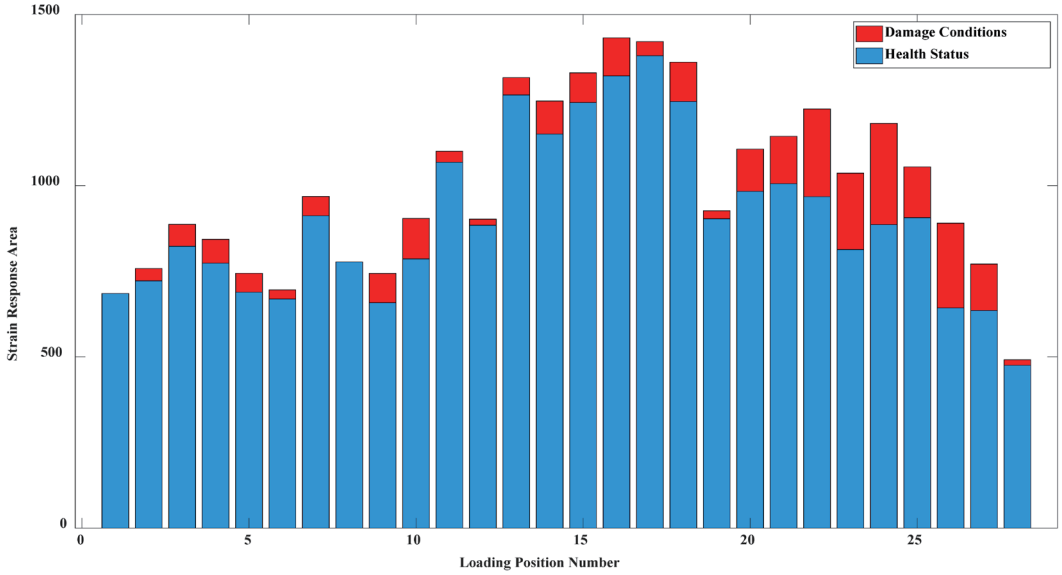

Fig. 11. (Color online) Schematic of damage quantification for Small Damage Condition 1.

4.2 Damage diagnosis in the case of a medium degree of damage

The test data of medium Damage Condition 3 of the disassembly of transverse connections #6 and #17 were selected for analysis. The front wheels of the loading vehicle were 90, 160, and 230 cm deep. As shown in Fig. 12, there was minimal difference in the relative strain relationship before and after damage to the structure, and it was impossible to determine whether the structure was damaged under these damage conditions. As shown in Fig. 13, after this algorithm, 10 damage indicators exceeded the threshold, which indicates that the structure was damaged.

The damage location area given by the damage diagnosis algorithm is 90–170 cm away from the right end of the bridge. The #6 and #17 horizontal connections are 128 cm away from the right end of the bridge, which is within the positioning range shown in Fig. 14.

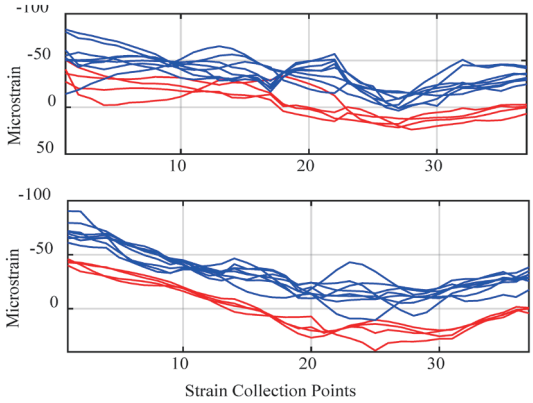

Fig. 12. (Color online) Damage Condition 3: Loading at 90 cm position of front wheel.

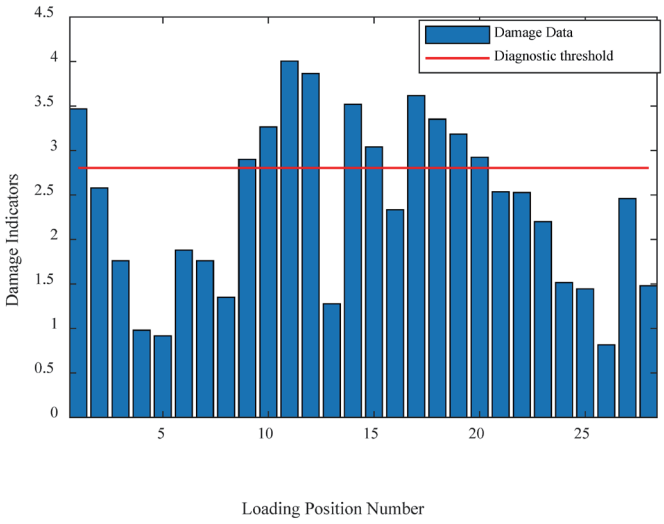

Fig. 13. (Color online) Damage diagnosis results for Damage Condition 3.

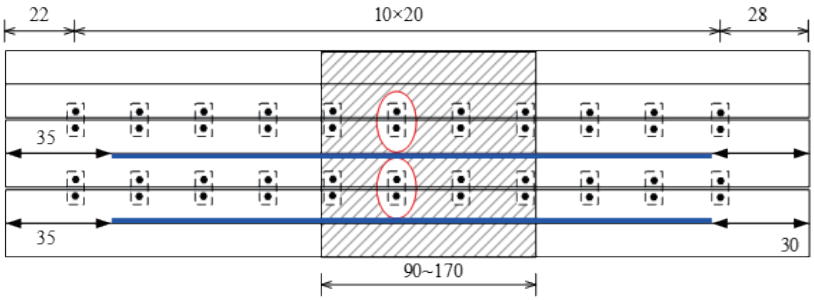

Fig. 14. (Color online) Relationship between damage location and lateral connection position for Working Condition 3 (unit: cm).

Working Condition 3 has an additional #17 transverse connection dismantled at the midspan position, which reduces the stiffness of the midspan section and causes a decrease in the structural stiffness of the nearby area. When the vehicle is loaded into the midspan area, the strain response area obtained at several loading points in the area increases relative to the healthy working condition; thus, the damage diagnosis index increases.

The damage quantification algorithm is used to quantify the damage under Damage Condition 7, and the results are shown in Fig. 15. The bridge damage quantification index φ = 0.124 obtained from the program results indicates that the degree of damage to the bridge structure occuring under Damage Condition 1 is 12.4%.

4.3 Damage diagnosis in the case of a large degree of damage

When the diagnostic algorithm of bridge structural damage is used to assess the damage of a large structure, the greater the amount of structural strain response data obtained under healthy conditions, the more stable the normal value of the structural strain under healthy conditions and the greater the accuracy of damage determination by comparing the structural strain response. For severe damage conditions, the #6, #7, #17, and #18 transverse connections were removed. The strain response curves of the structure before and after the damage were selected for loading at the 160 cm position of the front wheel, and the comparison diagram is shown in Fig. 16.

When the damage is severe, the displacement influence line method can directly determine whether the structure has been damaged, revealing the sensitivity of the proposed algorithm in the case of minor damage. This demonstrates that the Bragg frequency shift data collected using the BOTDA technology can accurately represent the changes in structural strain response. When using this algorithm to assess damage for large-scale structures, the more strain response data of

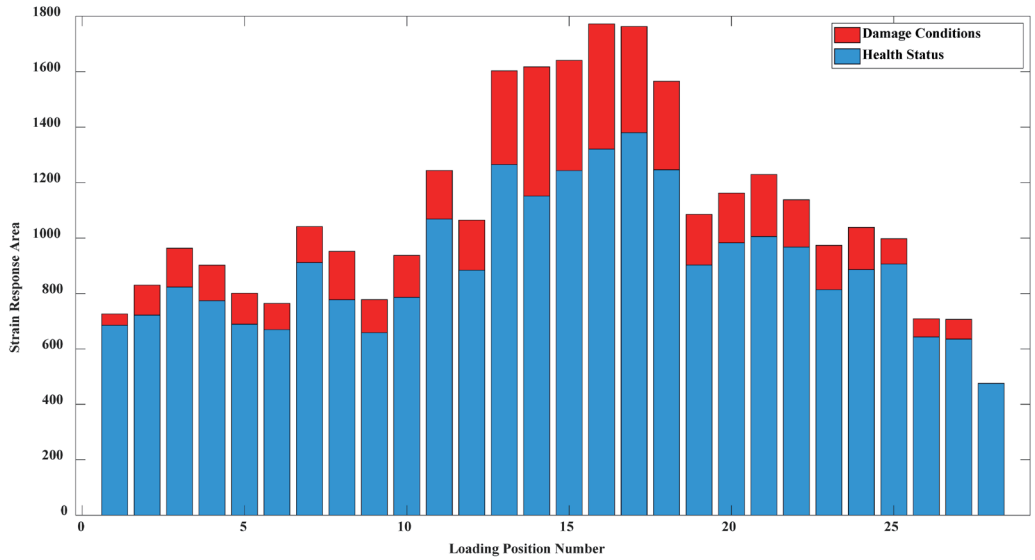

Fig. 15. (Color online) Quantitative damage results for Working Condition 3.

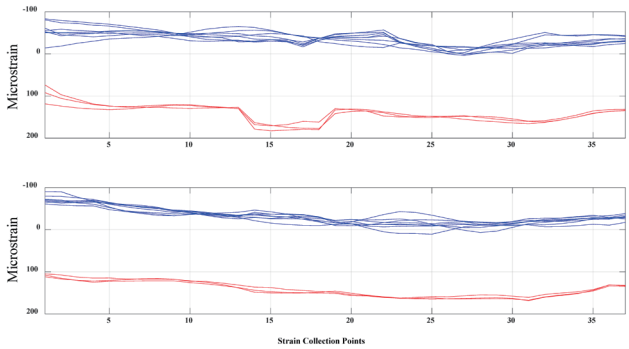

Fig. 16. (Color online) Damage Condition 4: Loading at 90 cm position of front wheel.

the structure obtained under a healthy condition, the more stable the normal strain values of the structure under healthy conditions will be. The accuracy of determining damage through comparison of the strain responses of the structure will be higher.

5. Conclusions

To address the problems of damage identification and location for small- and medium-span beam bridges, a diagnosis method based on DPP-BOTDA technology was proposed, which can simultaneously meet the requirements of structural damage identification, damage area location, and damage quantification. The main conclusions are as follows.

(1) Optical fiber sensing technology has high accuracy in bridge structure monitoring.
(2) For less damage, the proposed method has a better identification effect than the numerical method, which is based on quasistatic influence lines.
(3) The greater the amount of structural strain response relationship data obtained under healthy conditions, the more stable the normal value of the structural strain under healthy conditions and the greater the accuracy of damage determination when the structural strain response is compared.
(4) The proposed method is suitable for bridges for which an initial dataset of bridge health status can be established. For the existing damaged bridge structures, they first need to be reinforced to obtain the data under healthy conditions before they can be evaluated. The issues related to damage diagnosis for other bridge types and other parts still need further exploration and research.
(5) This algorithm is currently applicable to precast beam bridges. For other types of bridges, its applicability needs to be verified through practical tests before it can be considered. In a time-varying temperature environment, if the temperatures during the monitoring period are similar, this algorithm can be adopted.

Acknowledgments

This work was supported by the Engineering Construction Research Project of Zhejiang Provincial Department of Transportation (No. 2022-GCKY-03).

References

1 F. Abdoli, M. Rashidi, J. Wang, R. Siddique, and V. Nasir: Results Eng. **24** (2024) 103084. https://doi.org/10.1016/j.rineng.2024.103084
2 F. Fanian, M. K. Rafsanjani, and M. Shokouhifar: Appl. Soft Comput. **167** (2024) 112429. https://doi.org/10.1016/j.asoc.2024.112429
3 X. Yan, K. Wang, M. Gao, C. Li, and Y. Liu: J. Civil Struct. Health Monit. **15** (2025). https://doi.org/10.1007/s13349-025-00909-x
4 T. Q. Nguyen, T. B. Vu, N. Shafiabady, T. T. Nguyen, and P. T. Nguyen: Structures **70** (2024) 107733. https://doi.org/10.1016/j.istruc.2024.107733
5 W. Xu, Y. Gao, K. Wang, and N. Li: highway **69** (2024).
6 J. Yu, W. Wan, B. Xiang, J. Wen, Q. Zhan, and D. Wu: Heilongjiang Transp. Sci. Technol. **46** (2023) 64.
7 Y. Liu and M. Gao: Comput.-Aided Civ. Infrastruct. Eng. **37** (2022) 1891. https://doi.org/10.1111/mice.12874.
8 X. Li, F.-L. Zhang, W. Xiang, W.-X. Liu, and S.-J. Fu: Structures **70** (2024) 107739. https://doi.org/10.1016/j.istruc.2024.107739.
9 Y. Xu, W. Hong, M. Noori, W. A. Altabey, A. Silik, and N. S. D. Farhan: Struct. Durability Health Monit. **18** (2024) 763. https://doi.org/10.32604/sdhm.2024.053763.
10 C. Fan, Y. Zheng, B. Wang, Y. Zhou, and M. Sun: Mech. Syst. Signal Process. **200** (2023) 110518. https://doi.org/10.1016/j.ymssp.2023.110518.
11 Y. Liu and S. Zhang: Sensors **18** (2018). https://doi.org/10.3390/s18124446.
12 F. Deng, S. Wei, X. Jin, Z. Chen, and H. Li: Mech. Syst. Signal Process. **186** (2023) 109908. https://doi.org/10.1016/j.ymssp.2022.109908.
13 J. Zhu, C. Zhang, and X. Li: Measurement **211** (2023) 112599. https://doi.org/10.1016/j.measurement.2023.112599
14 Z. Zhou, Y. Liu, and H. Li: Measurement **211** (2023) 112611. https://doi.org/10.1016/j.measurement.2023.112611
15 Y. Liu, H. Li, Y. Wang, Y. Men, and Q. Xu: Mech. Syst. Signal Process. **158** (2021) 107728. https://doi.org/10.1016/j.ymssp.2021.107728
16 E. A. Oskoui, T. Taylor, and F. Ansari: Eng. Struct. **189** (2019) 385. https://doi.org/10.1016/j.engstruct.2019.02.037
17 F. Yang, X. Feng, J. Zhang, G. Zhong, and Y. Yuan: Tunnelling Underground Space Technol. **139** (2023) 105215. https://doi.org/10.1016/j.tust.2023.105215
18 L. Ying, C. Zhang, and G. Ying: Eng. Struct. **320** (2024) 118904. https://doi.org/10.1016/j.engstruct.2024.118904
19 L. Nguyen-Ngoc, H. Tran-Ngoc, T. Le-Xuan, C.-T. Nguyen, G. De Roeck, T. Bui-Tien, and M. Abdel Wahab: Adv. Eng. Software **198** (2024) 103795. https://doi.org/10.1016/j.advengsoft.2024.103795
20 X. Meng, D. Zhang, H. Li, and Y. Huang: Measurement **203** (2022) 111966. https://doi.org/10.1016/j.measurement.2022.111966
21 X. Wu, H. Feng, Z. Sha, J. Gao, H. Zhang, X. Rui, and Y. Zhang: Measurement **239** (2025) 115477. https://doi.org/10.1016/j.measurement.2024.115477
22 Z. Yu, M. Zhang, H. Dai, L. Liu, J. Zhang, X. Jin, and G. Wang: Opt. Laser Technol. **105** (2018) 89. https://doi.org/10.1016/j.optlastec.2018.02.037
23 C. Jiang, J. Ma, M. Li, H. Lu, X. Wen, and K. Su: Opt. Laser Technol. **143** (2021) 107361. https://doi.org/10.1016/j.optlastec.2021.107361
24 Y. Meng, J. Zha, and Y. Liu: Opt. Commun. **437** (2019) 219. https://doi.org/10.1016/j.optcom.2018.12.073
25 J. Li, K. Zeng, G. Yang, L. Wang, J. Mi, L. Wan, M. Tang, and D. Liu: Opt. Commun. **525** (2022) 128866. https://doi.org/10.1016/j.optcom.2022.128866